Letter

Unique d_{xy} superconducting state in the cuprate $Ba_2CuO_{3.25}$

Priyo Adhikary,[1,2] Mayank Gupta,[1,3] Amit Chauhan,[1,3] Sashi Satpathy,[3,4]
Shantanu Mukherjee,[1,2,*] and B. R. K. Nanda[1,3,†]

[1]*Center for Atomistic Modelling and Materials Design, Indian Institute of Technology Madras, Chennai 600036, India*
[2]*Department of Physics, Indian Institute of Technology Madras, Chennai 600036, India*
[3]*Condensed Matter Theory and Computational Lab, Department of Physics, Indian Institute of Technology Madras, Chennai 600036, India*
[4]*Department of Physics & Astronomy, University of Missouri, Columbia, Missouri 65211, USA*

(Received 28 February 2023; revised 7 October 2023; accepted 5 January 2024; published 22 January 2024)

Recent discovery of superconductivity at a transition temperature of 73 K in the doped layered compound Ba_2CuO_{3+x} for $x \sim 0.2$ has generated a lot of interest. Experiments in this alternately stacked oxygen octahedral and chain layered structure reveal that a compression of the octahedra causes the Cu-d_{z^2} orbital to lie above the Cu-$d_{x^2-y^2}$ orbital unlike in the well-known cuprate superconducting materials. Our first-principles calculations and low-energy Hamiltonian studies on the $x = 0.25$ system reveal that this energy ordering results in formation of d_{z^2}-dominated electron pockets. The strong nesting in the Fermi pockets leads to an AFM spin fluctuation mediated d_{xy}-wave superconducting state dominated by pairing among the d_{z^2} orbitals. This is in contrast to the cuprate superconductors (e.g., YBCO) where both electron and hole pockets exist and the superconducting state with B_{1g} symmetry are formed by the $d_{x^2-y^2}$ orbital electrons. Unlike the earlier reports we find the interlayer hybridization has an important contribution to the low-energy band structure and formation of the unconventional superconducting state.

DOI: 10.1103/PhysRevB.109.L020505

Introduction. A large class of cuprate compounds shows a high-temperature superconducting phase at moderate carrier doping, where Cu $d_{x^2-y^2}$ orbital electrons are responsible for the formation of the Cooper pair condensate. Recently a new class of overdoped cuprate material [1,2] has emerged, which exhibits higher superconducting transition temperature than the typical cuprates at similar carrier doping [3–5]. Among them is the orthorhombic compound Ba_2CuO_{3+x} [6] with a superconducting transition temperature of $T_c \sim 73$ K. In this material, an octahedral distortion breaks the degeneracy of the e_g orbitals, leading to a partially filled d_{z^2} orbital and a fully occupied $d_{x^2-y^2}$ orbital. The presence of high-temperature superconductivity in this material in spite of significantly higher doping levels and low-energy physics that is dominated by d_{z^2} orbitals provides a new channel for understanding high-temperature superconductivity. Recent experimental studies on Ba_2CuO_{3+x} with $x = 0.2$ [6,7] measuring oxygen K-edge x-ray absorption spectra (XAS) estimate 40% doping, which is significantly higher than doping in overdoped cuprates such as YBCO. The Zhang-Rice singlet state is observed at this oxygen doping with dominant prepeak at 528 eV photon energy [6]. The XAS measurements [6] on the $Ba_2CuO_{3.2}$ suggested a compressed octahedral structure. This prompted Maier *et al.* [8] to suggest a simplified two-band model using d_{z^2} and $d_{x^2-y^2}$ orbitals within the 214 structure. They propose two dome superconductivity, one at low doping and the other at high oxygen doping. Similar calculations based on spin-fluctuation theory on Lieb lattice [9] structure give $s\pm$ wave superconductivity.

The unit cell of $Ba_2CuO_{3.25}$ (BCO) has two layers, layer I and layer II (see Fig. 1). The DFT+DMFT-based calculations [10] proposed the presence of a charge transfer between layer I and layer II and proposed that due to the presence of a quasi-one-dimensional (quasi-1D) band, antiferromagnetic spin fluctuation may occur to give rise to superconductivity. The specific-heat measurement [6] on BCO indicates that superconductivity is very anisotropic in contrast to the exponential jump at T_c of conventional electron-phonon superconductivity.

In this Letter, using a combination of first-principles DFT calculations and a spin fluctuation mediated superconducting pairing mechanism [11], we find a crucial interlayer hybridization present in BCO, which not only helps to stabilize a novel d_{xy} symmetry superconducting state but also leads to a weak three-dimensional character to the superconducting gap function. Experimentally, in the XAS spectra, a transition $2p^6 3d^9 L \rightarrow 2p^5 3d^{10} L$ is seen [6], which we attribute to this hybridization and is associated with hopping between Cu-d and O-p_y/p_z orbitals. We identify the ground-state superconducting gap function for decoupled individual layers and the bulk BCO that includes interlayer hybridization. The analysis provides a comparative study between a layer decoupled and hybridized low-energy Hamiltonian to elucidate the role of the latter towards superconductivity. Despite the larger electronic doping, we find that the Fermi surface (FS) remains significantly nested, and it leads to a large paramagnetic susceptibility and superconducting pairing potential.

*shantanu@iitm.ac.in
†nandab@iitm.ac.in

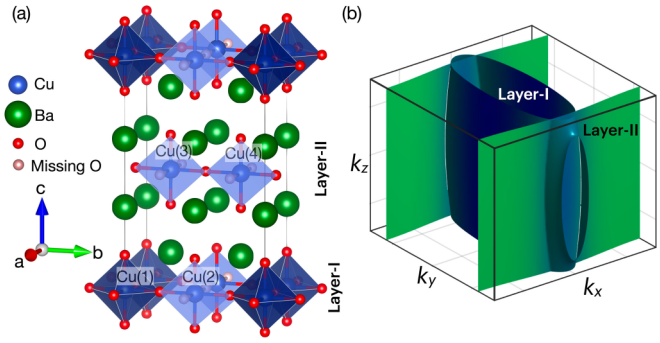

FIG. 1. (a) Crystal structure (Pmmm) of $Ba_2CuO_{3.25}$ (BCO). Layer I has alternate stacking of octahedral and square planar Cu-O complexes (along *b*). The octahedra form a corner-share network along *a* direction. In layer II, due to missing oxygen atoms when compared to Ba_2CuO_4, only square planar complexes exist and they form a chain along *b* direction. (b) The Fermi surface of BCO. Center elliptical pocket with strong nesting is formed by Cu(1)-d_{z^2} orbital of layer I while the open electron sheets are formed by Cu(3, 4)-$d_{b^2-c^2}$ layer II.

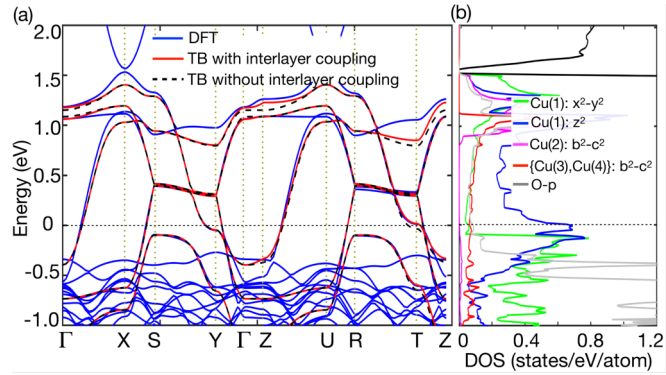

FIG. 2. (a) The five-band TB model fitted with DFT bands with and without interlayer coupling. The interlayer hybridization shifts the van Hove singularities near *Y* and *T* points at the high symmetry *k* path of the Brillouin zone. The energy gap between van Hove singularities is absent for the decoupled individual layers. The high symmetry *k* path used to plot the band structure is provided in the Fig. S1 of the SM [12]. (b) DFT obtained partial density of states.

The obtained superconducting gap function belongs to pairing between electrons predominantly in d_{z^2} orbitals.

We find that the gap symmetry and the strength of the pairing of the bulk are different from a model incorporating decoupled layers. Furthermore, due to the presence of interlayer hybridization, the magnitude of pairing eigenfunction has a weak k_z dependence, which is otherwise absent in the case of decoupled layers. The pairing symmetry of the bulk has a gap function with d_{xy} symmetry and the pairing symmetry of individual layer I is $s+$ type and layer II is s type with additional nodes at the FS. Further, the broken C_4 rotational symmetry due to structural distortion results in a pairing symmetry belonging to the D_{2h} point group.

Electronic structure. Employing the DFT+DMFT method, Worm *et al.* [10] have examined the electronic structure of BCO to make a broad prediction of the presence of an almost half-filled, strongly nested, quasi-1D $d_{b^2-c^2}$ band, which is probable cause of superconductivity. Here, we would like to make a comprehensive analysis of the electronic structure using DFT and to develop a tight-binding (TB) model that examines the interlayer coupling and its effect on FS of the BCO. As discussed later and in the Supplemental Material (SM) [12], the minimal basis set TB model is developed by both the Slater-Koster formulation and the Löwdin down-folding technique.

The DFT-derived bands are shown in blue in Fig. 2(a), along with the orbital-resolved density of states shown in Fig. 2(b). Details of the DFT calculations and orbital-resolved band structure are provided in the SM [12] (see also Refs. [1–5] therein). Below we mention the main findings of DFT results. (i) d_{z^2} orbital of Cu(1) is within the range of -0.56 eV to 1.13 eV with respect to the Fermi level (E_F). The $d_{x^2-y^2}$ orbital is completely occupied and lies in the range -1.57 eV to -0.09 eV. This highlights the role of d_{z^2} orbitals in the typical energy scales associated with the superconducting transition. (ii) $d_{b^2-c^2}$ orbital of Cu(2) is about 0.89 eV above E_F (0.89–1.56 eV). (iii) The O-p states are extended in valence bands and lie up to -0.27 eV below E_F.

To gain further insight into the electronic structure, specifically to obtain the eigenvectors of the states occupying the Fermi level, we developed a low-energy TB Hamiltonian initially with a 14 orbital basis and later down folded to a five-orbital basis. The Hamiltonian reproduces well the DFT band structure in the corresponding energy range [see Fig. 2(a)] and thereby enables us to calculate the random phase approximation (RPA) spin susceptibility.

In this model, four Cu atoms in the unit cell contribute five Cu-d orbitals, and the nearest-neighbor O atoms contribute to the nine O-p orbitals near the Fermi level (see SM [12] for detailed analysis). We write the Hamiltonian in the following form,

$$H = \sum_{\alpha\beta} \sum_{\substack{\mathbf{k} \\ \sigma\in(\uparrow,\downarrow)}} [\xi_{\alpha\beta}(\mathbf{k}) + \mu_\alpha \delta_{\alpha\beta}] c^\dagger_{\mathbf{k},\alpha,\sigma} c_{\mathbf{k},\beta,\sigma}. \quad (1)$$

Here, $c^\dagger_{\mathbf{k},\alpha,\sigma}$ ($c_{\mathbf{k},\alpha,\sigma}$) is the fermion creation (annihilation) operator for orbital α with spin $\sigma = \uparrow, \downarrow$. $\xi_{\alpha\beta}(\mathbf{k})$ is the kinetic energy term containing hopping parameters and μ_α is the on-site energy.

Since there are two weakly coupled inequivalent layers in the system, the TB Hamiltonian contains intralayer and interlayer Hamiltonian contributions. In a matrix form, the Hamiltonian can be expressed as:

$$H = \begin{pmatrix} H_{l1} & H_{l1-l2} \\ H^\dagger_{l1-l2} & H_{l2} \end{pmatrix}. \quad (2)$$

Here, H_{l1} and H_{l2} are the intralayer Hamiltonian submatrices for layer I and layer II respectively, and H_{l1-l2} accounts for the interlayer hybridization. Using Löwdin down-folding [18] procedure, we obtain an effective Hamiltonian by integrating out the oxygen subspace while keeping only the Cu-d orbitals in the Hamiltonian. The matrix elements and the down-folding formalism are provided in the SM [12].

The TB bands with and without interlayer hybridization are shown in Fig. 2(a) and are compared with the DFT-obtained band structure. The lack of interlayer coupling does not

reproduce the band structure well with the subtle differences seen in Fig. 2(a) when momenta changes along $T(0,\pi,\pi)$ to $Z(0,0,\pi)$ direction. The distinction between them comes from interlayer hybridizations Cu(1)-d–Cu(3, 4)-d of strength $t_{12}^{(1)}$ and between Cu(1)-d–O-p of strength $t_{12}^{(2)}$. We find $t_{12}^{(1)}$ to be one order of magnitude higher than $t_{12}^{(2)}$ (see SM [12]). Most importantly, the interlayer hopping pushes the van Hove singularity slightly above the Fermi level. The d_{z^2} orbital of Cu(1) and $d_{b^2-c^2}$ orbital of Cu(3, 4) cross Fermi level and form electronlike pockets. Both electron pockets hybridize near $Y(0,\pi,0)$ point. The $d_{x^2-y^2}$ orbital of Cu(1) octahedra lies slightly below the Fermi level. This happens because of octahedral distortion in the BCO structure at very high doping. We can see in Fig. 2(b) that Cu(1)-d_{z^2} and Cu(3, 4)-$d_{b^2-c^2}$ have larger DOS at the E_F than Cu(2)-d orbitals. The FS topology of the bulk is shown in Fig. 1(b).

Superconducting state. The multiorbital superconducting pairing kernel is derived from a spin fluctuation pairing mechanism [4,5,19–38]. The fluctuation exchange approximation (FLEX) that has been successfully utilized to extract the ground-state superconducting states of both cuprate [4,5,19–26] and iron-based superconductors [4,5,27–31]. The pairing kernel involves contribution from paramagnetic and charge susceptibilities that are calculated from a Hubbard-Hund Hamiltonian within the RPA (see SM [12] for detailed analysis). Finally, the pairing interaction is included in the self-consistent linearized gap equation in order to extract the ground-state superconducting gap functions. The gap equation reads,

$$\Delta_\nu(\mathbf{k}) = -\lambda \frac{1}{\Omega_{BZ}} \sum_{\nu',\mathbf{q}} \Gamma'_{\nu\nu'}(\mathbf{k},\mathbf{q})\Delta_{\nu'}(\mathbf{k}+\mathbf{q}), \tag{3}$$

where $\Gamma'_{\nu\nu'}(\mathbf{k},\mathbf{q})$ is SC pairing potential and λ is the pairing strength. We obtain SC pairing potential by expanding the interaction term of the Hubbard Hamiltonian in a perturbation series and collecting the bubble and ladder diagrams,

$$\tilde{\Gamma}_s(\mathbf{q}) = \tfrac{1}{2}[3\tilde{U}_s\tilde{\chi}_s(\mathbf{q})\tilde{U}_s - \tilde{U}_c\tilde{\chi}_c(\mathbf{q})\tilde{U}_c + \tilde{U}_s + \tilde{U}_c]. \tag{4}$$

Here, $\chi_s(\chi_c)$ is the RPA spin (charge) susceptibility.

In BCO, the effect of a broken C_4 rotational symmetry can be seen on the FS and corresponding spin susceptibility calculations. We first explore the Hamiltonian in the limit of no interlayer hybridization. In Figs. 3(a) and 3(b) we show the FS topology of layer I and layer II, respectively, at $k_z = 0$. We find that layer I shows a stronger 2D dispersion as compared to layer II. The effect of the quasi-1D nature of layer II shows up in the 1D susceptibility peaks observed from its FS nesting. The dominant FS nesting vectors for individual layers are also shown in Figs. 3(a) and 3(b). We show the spin susceptibility of layer I and layer II in Figs. 3(c) and 3(d), respectively. This chainlike 1D FS enhances spin susceptibility in each layer for small values for Hubbard interactions and leads to a dominant nesting for layer II at the incommensurate wave vector $\mathbf{Q_2} = (\pm 0.96\pi, \pm 0.68\pi)$. Similarly, the spin susceptibility result of layer I leads to a corresponding peak at $\mathbf{Q_1} = (\pm 0.66\pi, 0)$. We find that χ_s at $\mathbf{Q_2}$ is larger than the corresponding maximum for $\mathbf{Q_1}$.

When interlayer hybridization is absent, SC of each layer is decoupled from the bulk BCO. Peaks of spin susceptibility

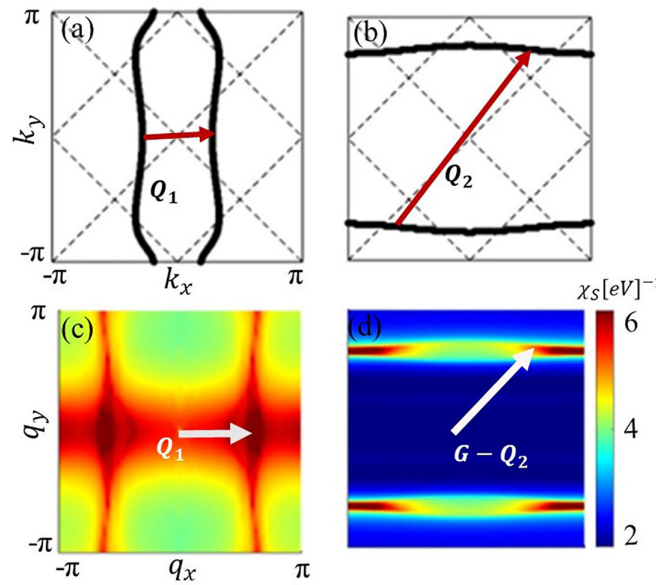

FIG. 3. (a), (b) Fermi surfaces of decoupled individual layer I and layer II in k_x-k_y plane. The Fermi pockets are electronlike, coming from the d_{z^2} orbital of Cu(1) atom and $d_{b^2-c^2}$ orbital of Cu(3) atom. (c), (d) RPA spin susceptibility [Tr[χ_s]] of decoupled individual layer I and layer II within the q_x-q_y plane. The dominant nesting vectors are denoted by $\mathbf{Q_1}$, $\mathbf{Q_2}$. $\mathbf{G}$ is the reciprocal lattice vector.

will determine the maximum pairing potential when nesting condition ($\xi_{\mathbf{k}+\mathbf{Q}} = -\xi_{\mathbf{k}}$) is satisfied by the momentum $\mathbf{q} = \mathbf{Q}$ at the FS. The strong deviation of the dominant susceptibility from the C_4 susceptibility of the well-known cuprates can lead to corresponding deviations in the superconducting state. We plot the superconducting gap function for layer I and layer II for the largest pairing eigenvalue in Figs. 4(a) and 4(b), respectively. Color map blue to red denotes the sign of the pairing symmetry. The pairing symmetry of layer I and layer II leads to a dominant spin singlet superconducting gap that would transform as an A_{1g} irreducible representation of the D_{2h} point group symmetry. Whereas for layer I the gap is only anisotropic near the region of large curvature of the FS, the

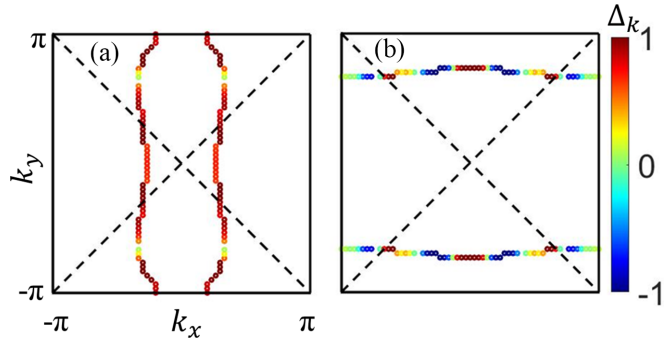

FIG. 4. (a), (b) The superconducting pairing eigenfunction for the largest eigenvalue on the Fermi surface for decoupled individual layer I and layer II, respectively. The pairing symmetry of layer I and layer II belongs to A_{1g} irreducible representation of the D_{2h} point group.

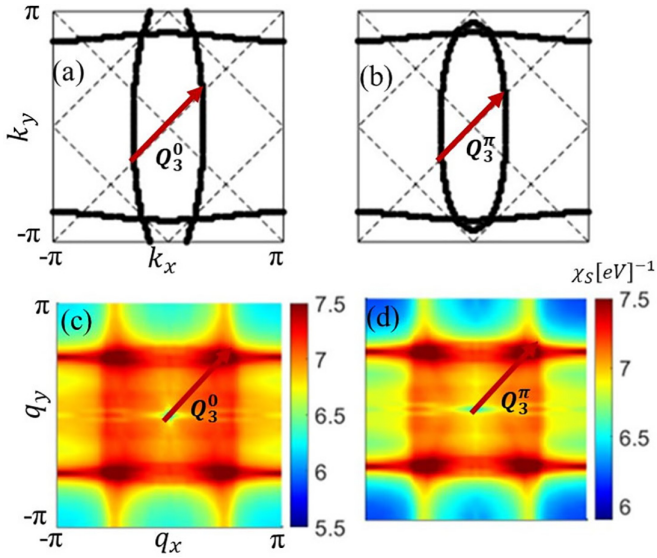

FIG. 5. (a), (b) The Fermi surface of BCO in the presence of interlayer hybridization at two different k_z values. The weak 3D dispersion induced by the interlayer hybridization causes ellipticity of the electron pocket at $k_z = \pi$ as compared to the pocket at $k_z = 0$. (c), (d) RPA spin susceptibility, Tr$[\chi_s]$ for two q_z values. The dominant nesting vectors are denoted by $\mathbf{Q_3^0}$, $\mathbf{Q_3^\pi}$.

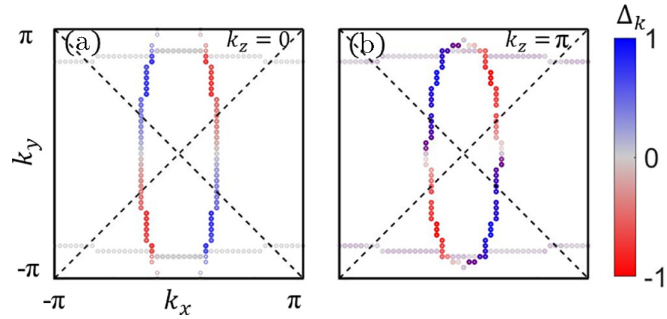

FIG. 6. (a), (b) The solution of the superconducting gap equation on the Fermi surface of the bulk BCO for two representatives k_z values. The pairing symmetry in presence of interlayer hybridization is d_{xy} type with nodes along the $k_x = 0$ and $k_y = 0$ lines on the Fermi surface.

gap on layer II shows the presence of accidental nodes. We also find that the superconducting gaps have a 2D structure over the FS within negligible k_z dispersion.

The formation of a SC gap with A_{1g} symmetry despite of a repulsive pairing interaction is explained by the dominance of the interorbital pairing channel over the intraorbital pairing contribution (see the discussion in Sec. IV of SM [12]). This large off-diagonal contribution leads to an attractive pairing. Such a scenario can also be induced by Hund's interaction [39], although for BCO it is already present at the noninteracting level.

We next include interlayer hybridization in the noninteracting Hamiltonian. In Figs. 5(a) and 5(b) we show the FS of bulk BCO at $k_z = 0$ and $k_z = \pi$, respectively. Interestingly, the interlayer hybridization not only enhances the dispersion of the electronic bands along the k_z direction, it also leads to a significant shift of the dominant susceptibility peak. The RPA spin susceptibility at $q_z = 0$, and $q_z = \pi$ are shown in Figs. 5(c) and 5(d). As shown in Fig. 5(c), the dominant nesting vector is still in the k_x-k_y plane but leads to a susceptibility peak at the wave vector $\mathbf{Q_3^0} = (\pm 0.48\pi, \pm 0.52\pi)$ for $k_z = 0$. The larger ellipticity of the electron pocket at $k_z = \pi$ as compared to the pocket at $k_z = 0$ shows the weak 3D dispersion induced by the interlayer hybridization, and as shown in Fig. 5(d) leads to a susceptibility peak at around $\mathbf{Q_3^\pi} = (\pm 0.44\pi, \pm 0.56\pi)$ wave vector.

The effect of interlayer hybridization is even more significant for the ground-state superconducting gap functions. In Figs. 6(a) and 6(b) we plot the superconducting gap function of bulk BCO for the largest pairing eigenvalues at two different k_z values. The pairing symmetry of bulk BCO on the elliptical hole pocket can be expressed in the form $\Delta(\mathbf{k}) = \Delta_0 \sin(k_x) \sin(k_y)$ with line nodes along the $k_x = 0$ and $k_y = 0$ lines on the FS. This is similar to the cuprate B_{1g} superconducting basis function on a $\pi/4$ rotated axis. We find that although the sign of the gap remains unchanged along k_z, the gap function magnitude (Δ_0) gets enhanced with increasing k_z. In bulk BCO, the pairing eigenvalue λ seems to closely track the transition of unhybridized layer I model (see SM [12] Fig. S4). This feature is likely due to the dominance of the d_{z^2} electrons and corresponding orbital resolved pairing interaction for the layer I model. Our predictions can be probed by experimental techniques such as ARPES, STM among a variety of techniques that have been successfully utilized to understand the superconducting state in the cuprates.

Conclusions. The recent discovery of superconductivity in BCO at $T_c = 73$ K with high hole doping levels places this material in a new parameter regime among the various classes of cuprate high-temperature superconductors. From the DFT calculations, we find that the d_{z^2} orbital of the Cu(1) atom belonging to the octahedra lies at the Fermi level, and $d_{x^2-y^2}$ orbital is fully occupied. This makes BCO different from usual cuprate superconductors. We propose an effective five-orbital tight-binding model consisting of the selective d orbitals of the Cu atoms that shows excellent agreement with the DFT band structure when an interlayer hybridization is included in the model. From the tight-binding analysis, we find the hybridization between the BCO layers, albeit weak, significantly influences the band structure along $Y\Gamma$ and TZ where the van Hove singularities exist. The d orbitals coming from Cu(3)[Cu(4)] and Cu(1) atoms form electronlike pocket at the Fermi level. Similar to the YBCO, the planar layer of bulk BCO forms quasi-1D chain states. However, the hole pocket coming from $d_{x^2-y^2}$ orbital in YBCO [40] and infinite layer nickelates [41] are absent in BCO.

In BCO, the presence of interlayer hybridization plays a pivotal role in reshaping the Fermi surface. It removes the parallel Fermi pocket regions connected by dominant interorbital contributions. This leads to the dominance of intraorbital nesting and susceptibility along the $(\pi - \delta, 0)$ wave vector (see SM [12], Sec. S IV for orbital resolved susceptibility contributions. This diagonal intraorbital pairing contribution will support an unconventional superconducting order. Additionally, the $(\pi - \delta, 0)$ nesting wave vector found

in our susceptibility calculations would support d_{xy} symmetry superconducting order. We find an *s*-wave gap on Fermi pocket (without sign changeover) for layer I, if we ignore the interlayer hybridization. However, for layer II, we do find a sign change of the superconducting gap over the Fermi pocket that is expected from repulsive interaction. Therefore, the gap over the entire Fermi pocket should not be considered as a conventional *s*-wave gap but belonging to A_{1g} symmetry with higher harmonic contributions that can lead to a sign change of gap on layer II. The signatures of the nodal sign changing d_{xy} gap can be probed in future thermodynamic measurements such as low-temperature specific heat and thermal conductivity measurements. With synthesis of good quality single crystals, the gap should also be directly observable in ARPES and scanning tunneling spectroscopic experiments.

Acknowledgments. This work is funded by Science and Engineering Research Board of Department of Science and Technology (SERB-DST), India through Grant No. CRG/2020/004330. S.S. thanks SERB-DST, India for the Visiting Advanced Joint Research (VAJRA) program. S.M. acknowledges the financial support by SERB-DST, India through the MATRICS Grant No. MTR/2020/000524.

[1] Q. Q. Liu, H. Yang, X. M. Qin, Y. Yu, L. X. Yang, F. Y. Li, R. C. Yu, C. Q. Jin, and S. Uchida, Enhancement of the superconducting critical temperature of $Sr_2CuO_{3+\delta}$ up to 95 K by ordering dopant atoms, Phys. Rev. B **74**, 100506(R) (2006).

[2] A. Gauzzi, Y. Klein, M. Nisula, M. Karppinen, P. K. Biswas, H. Saadaoui, E. Morenzoni, P. Manuel, D. Khalyavin, M. Marezio, and T. H. Geballe, Bulk superconductivity at 84 K in the strongly overdoped regime of cuprates, Phys. Rev. B **94**, 180509(R) (2016).

[3] A. Damascelli, Z. Hussain, and Z.-X. Shen, Angle-resolved photoemission studies of the cuprate superconductors, Rev. Mod. Phys. **75**, 473 (2003).

[4] D. J. Scalapino, A common thread: The pairing interaction for unconventional superconductors, Rev. Mod. Phys. **84**, 1383 (2012).

[5] K. H. Bennemann and J. B. Ketterson, *Superconductivity: Conventional and Unconventional Superconductors* (Springer, Berlin, 2008), p. 3.

[6] W. M. Li, J. F. Zhao, L. P. Cao, Z. Hu, Q. Z. Huang, X. C. Wang, Y. Liu, G. Q. Zhao, J. Zhang, Q. Q. Liu, R. Z. Yu, Y. W. Long, H. Wu, H. J. Lin, C. T. Chen, Z. Li, Z. Z. Gong, Z. Guguchia, J. S. Kim, G. R. Stewart *et al.*, Superconductivity in a unique type of copper oxide, Proc. Natl. Acad. Sci. USA **116**, 12156 (2019).

[7] R. Fumagalli, A. Nag, S. Agrestini, M. Garcia-Fernandez, A. C. Walters, D. Betto, N. B. Brookes, L. Braicovich, K.-J. Zhou, G. Ghiringhelli, and M. Moretti Sala, Crystalline and magnetic structure of Ba_2CuO_3 investigated by x-ray absorption spectroscopy and resonant inelastic x-ray scattering, Physica C: Supercond. Appl. **581**, 1353810 (2021).

[8] T. Maier, T. Berlijn, and D. J. Scalapino, Two pairing domes as Cu^{2+} varies to Cu^{3+}, Phys. Rev. B **99**, 224515 (2019).

[9] K. Yamazaki, M. Ochi, D. Ogura, K. Kuroki, H. Eisaki, S. Uchida, and H. Aoki, Superconducting mechanism for the cuprate $Ba_2CuO_{3+\delta}$ based on a multiorbital lieb lattice model, Phys. Rev. Res. **2**, 033356 (2020).

[10] P. Worm, M. Kitatani, J. M. Tomczak, L. Si, and K. Held, Hidden one-dimensional, strongly nested, and almost half-filled Fermi surface in Ba_2CuO_{3+y} superconductors, Phys. Rev. B **105**, 085110 (2022).

[11] D. J. Scalapino, The case for pairing in the cuprate superconductors, Phys. Rep. **250**, 329 (1995).

[12] See Supplemental Material at http://link.aps.org/supplemental/10.1103/PhysRevB.109.L020505 for comprehensive discussions on the electronic structure calculations. Figure S1 show the BZ of BCO along with high symmetry points. Figure S2 presents the orbital-resolved DFT band structure along these high symmetry directions. Figure S3 compares the TB and fitted DFT band structures for the individual layers. Figure S4 illustrates the variation of the superconducting pairing eigenvalue with respect to the on-site Hubbard interaction for both individual layers and the bulk BCO. Figure S5 depicts the orbital-resolved Lindhard susceptibility in the absence of interlayer hybridizations. Lastly Fig. S6 shows the orbital-resolved Lindhard susceptibility alongside the orbital-resolved Fermi surfaces. It also contains Refs. [4,6,13–18,21–23,25–27,29–31,34–39].

[13] G. Kresse and J. Furthmüller, Efficient iterative schemes for *ab initio* total-energy calculations using a plane-wave basis set, Phys. Rev. B **54**, 11169 (1996).

[14] G. Kresse and D. Joubert, From ultrasoft pseudopotentials to the projector augmented-wave method, Phys. Rev. B **59**, 1758 (1999).

[15] P. E. Blöchl, Projector augmented-wave method, Phys. Rev. B **50**, 17953 (1994).

[16] J. P. Perdew, K. Burke, and M. Ernzerhof, Generalized gradient approximation made simple, Phys. Rev. Lett. **77**, 3865 (1996).

[17] J. C. Slater and G. F. Koster, Simplified LCAO method for the periodic potential problem, Phys. Rev. **94**, 1498 (1954).

[18] P.-O. Löwdin, A note on the quantum-mechanical perturbation theory, J. Chem. Phys. **19**, 1396 (1951).

[19] D. J. Scalapino, E. Loh, Jr., and J. E. Hirsch, *d*-wave pairing near a spin-density-wave instability, Phys. Rev. B **34**, 8190(R) (1986).

[20] T. M. Rice and K. Ueda, Gutzwiller method for heavy electrons, Phys. Rev. B **34**, 6420 (1986).

[21] J. R. Schrieffer, *Theory of Superconductivity* (W. A. Benjamin, New York, 1964).

[22] J. R. Schrieffer, X. G. Wen, and S. C. Zhang, Dynamic spin fluctuations and the bag mechanism of high-T_c superconductivity, Phys. Rev. B **39**, 11663 (1989).

[23] P. Monthoux, A. V. Balatsky, and D. Pines, Toward a theory of high-temperature superconductivity in the antiferromagnetically correlated cuprate oxides, Phys. Rev. Lett. **67**, 3448 (1991).

[24] M. Sigrist and K. Ueda, Phenomenological theory of unconventional superconductivity, Rev. Mod. Phys. **63**, 239 (1991).

[25] J. C. S. Davis and D.-H. Lee, Concepts relating magnetic interactions, intertwined electronic orders, and strongly correlated superconductivity, Proc. Natl. Acad. Sci. USA **110**, 17623 (2013).

[26] T. Das, R. Markiewicz, and A. Bansil, Intermediate coupling model of the cuprates, Adv. Phys. **63**, 151 (2014).

[27] I. I. Mazin, D. J. Singh, M. D. Johannes, and M. H. Du, Unconventional superconductivity with a sign reversal in the order parameter of $LaFeAsO_{1-x}F_x$, Phys. Rev. Lett. **101**, 057003 (2008).

[28] S. Graser, T. A. Maier, P. J. Hirschfeld, and D. J. Scalapino, Near-degeneracy of several pairing channels in multiorbital models for the Fe pnictides, New J. Phys. **11**, 025016 (2009).

[29] Z.-J. Yao, J.-X. Li, and Z. D. Wang, Spin fluctuations, interband coupling and unconventional pairing in iron-based superconductors, New J. Phys. **11**, 025009 (2009).

[30] T. Das and A. V. Balatsky, Stripes, spin resonance, and nodeless d-wave pairing symmetry in Fe_2Se_2-based layered superconductors, Phys. Rev. B **84**, 014521 (2011).

[31] A. Chubukov, Pairing mechanism in Fe-based superconductors, Annu. Rev. Condens. Matter Phys. **3**, 57 (2012).

[32] T. Takimoto, T. Hotta, and K. Ueda, Strong-coupling theory of superconductivity in a degenerate hubbard model, Phys. Rev. B **69**, 104504 (2004).

[33] T. Das, J.-X. Zhu, and M. J. Graf, Theory of nodal s±-wave pairing symmetry in the Pu-based 115 superconductor family, Sci. Rep. **5**, 8632 (2015).

[34] H. Ikeda, M.-T. Suzuki, and R. Arita, Emergent loop-nodal $s_{\pm}$-wave superconductivity in $CeCu_2Si_2$: Similarities to the iron-based superconductors, Phys. Rev. Lett. **114**, 147003 (2015).

[35] T. Nomoto and H. Ikeda, Exotic multigap structure in UPt_3 unveiled by a first-principles analysis, Phys. Rev. Lett. **117**, 217002 (2016).

[36] T. Nomoto and H. Ikeda, Symmetry-protected line nodes in non-symmorphic magnetic space groups: Applications to UCoGe and UPd_2Al_3, J. Phys. Soc. Jpn. **86**, 023703 (2017).

[37] J. Schmalian, Pairing due to spin fluctuations in layered organic superconductors, Phys. Rev. Lett. **81**, 4232 (1998).

[38] G. Saito and Y. Yoshida, Organic superconductors, Chem. Rev. **11**, 124 (2011).

[39] M. Roig, A. T. Rømer, A. Kreisel, P. J. Hirschfeld, and B. M. Andersen, Superconductivity in multiorbital systems with repulsive interactions: Hund's pairing versus spin-fluctuation pairing, Phys. Rev. B **106**, L100501 (2022).

[40] P. Adhikary and T. Das, Prediction of f-wave pairing symmetry in $YBa_2Cu_3O_{6+x}$ cuprates, Phys. Rev. B **101**, 214517 (2020).

[41] P. Adhikary, S. Bandyopadhyay, T. Das, I. Dasgupta, and T. Saha-Dasgupta, Orbital-selective superconductivity in a two-band model of infinite-layer nickelates, Phys. Rev. B **102**, 100501(R) (2020).